Determination of Non-linear Damping Coefficients of bottom-hinged Oscillating Wave Surge Converters Using Numerical Free Decay Tests

H. Asmuth
Technische Universität Hamburg-Harburg, Hamburg, Germany

P. Schmitt & B. Elsaesser
Marine Research Group, School of Planning, Architecture and Civil Engineering
Queen's University Belfast, Belfast, United Kingdom

A. Henry
Aquamarine Power Ltd., Edinburgh, United Kingdom.

ABSTRACT: Linear wave theory models are commonly applied to predict the performance of bottom-hinged oscillating wave surge converters (OWSC) in operational sea states. To account for non-linear effects, the additional input of coefficients not included in the model itself becomes necessary. In ocean engineering it is common practice to obtain damping coefficients of floating structures from free decay tests.
This paper presents results obtained from experimental tank tests and numerical computational fluid dynamics simulations of OWSC's. Agreement between numerical and experimental methods is found to be very good, with CFD providing more data points at small amplitude rotations.
Analysis of the obtained data reveals that linear quadratic-damping, as commonly used in time domain models, is not able to accurately model the occurring damping over the whole regime of rotation amplitudes. The authors conclude that a hyperbolic function is most suitable to express the instantaneous damping ratio over the rotation amplitude and would be the best choice to be used in coefficient based time domain models.

1 INTRODUCTION

1.1 *Performance modeling of wave energy converters*

An overall techno-economical evaluation of flap-type oscillating wave surge converters (OWSC) requires the prediction of the annual power production. The local wave climate at a specific site is therefore simulated using numerical linear wave theory models and statistical wave occurrence data (Folley et al. 2009). Time domain data of incident waves is then fed into a hydrodynamic response model of the device. Underlying hydrodynamic parameters of the device's response are therefore provided in look-up tables and stem from supplementary linear numerical simulations or wave tank tests (van't Hoff 2009).

A description of the hydrodynamic response of a flap-type OWSC in the time domain can be given by

$$T_w = (I + I_a)\,\ddot{\theta} + k_p \sin\theta + d_r \cdot \dot{\theta} + d_{nl} \cdot \dot{\theta}|\dot{\theta}| + T_{PTO} \quad , \tag{1}$$

where T_w is the incident wave torque, θ the rotation angle of the device, I and I_a the inertia and added inertia, respectively, k_p the hydrodynamic pitch stiffness, d_r the damping due to wave radiation, d_{nl} the non-linear damping due to viscous effects and T_{PTO} the damping torque applied by the power take-off mechanism (PTO). Based on linear potential theory, commonly applied tools like *WAMIT* can not be used to determine non-linear viscous effects. Neither can wave tank tests since detailed near flow field analysis' of OWSCs are not straightforward (Osterried 2010). Thus the effects of non-linear damping are usually derived from the deviations of the modelled performance from the measured performance in wave tank tests.

Simulations of OWSCs using computational fluid dynamics (CFD) implicitly capture non-linear effects as they directly model the device and the surrounding fluid. They have been proven to accurately model the hydrodynamic response of wave energy converters (WEC) and allow detailed insights into their near flow field (Schmitt 2013, Bhinder et al. 2012). Still, their

application is limited to model several wave cycles of operation since computational costs are immense. Hence the prediction of the annual power production relies on simple models mentioned above and the explicit knowledge of underlying hydrodynamic parameters dependent on wave height and period (Schmitt et al. 2012).

In offshore engineering and naval architecture it is common practice to determine damping coefficients, both linear and non-linear, from free decay tests (Faltinsen 2010). With its only degree of freedom being pitch a free decay test of an OWSC is performed by displacing it from vertical in still water and releasing it. With no PTO damping applied ($T_{PTO} = 0$) and no waves present ($T_w = 0$), the OWSC consequently oscillates at its damped natural period, driven by its own restoring buoyancy moment $T_{kp} = k_p \cdot sin(\theta)$, as given in equation 1. According to the existing model the OWSC thereby experiences a linear damping torque due to wave radiation as well as a quadratic damping torque due to viscous losses, resulting in a decay of the oscillation. If the damping of a body is constant over the amplitude of the oscillation, generally valid, constant damping coefficients can be determined from the peak-to-peak decay of the oscillation. The latter unfortunately does not pertain to OWSCs (Henry 2009, van't Hoff 2009).

This paper presents the ongoing work on the determination of non-linear damping coefficients for OWSCs from free decay tests. Simulations of free decay tests in CFD are presented as well as their validation against experimental results. Furthermore the advantages of numerical free decay tests will be discussed. With respect to the operation of OWSCs the application of existing methods to gain damping coefficients from free decay tests is evaluated and compared to preceding research. Apart from the determination necessary steps towards implementing damping coefficients into existing models are discussed. Furthermore an outlook is given how to improve the presented approaches and corroborate the validation of the numerical method as part of future research.

1.2 *Mechanical Description of the Free Decay*

When released from an initial angle of displacement the period of oscillation of a damped body T_d can be described as

$$T_d = T_0 \cdot (1 - \zeta^2)^{-\frac{1}{2}} \quad . \tag{2}$$

where T_0 is the undamped natural period. The period of oscillation during the free decay consequently changes if the damping ratio ζ (ratio of the actual damping coefficient to the critical damping coefficient) is not constant during the decay or if the overall damping is generally non-linear. In order to analyse the damping during a free decay test with non-linear damping the logarithmic decrement method is usually applied (Inman 2008, Ikeda 1983). The equation of motion for the free decay, given by

$$0 = \ddot{\theta} + k'_p \cdot \sin\theta + d'_r \cdot \dot{\theta} + d'_{nl} \cdot \dot{\theta}|\dot{\theta}| \tag{3}$$

is therefore linearised which results in

$$0 = \ddot{\theta} + k'_p \cdot \theta + d'_e \cdot \dot{\theta} \qquad , \tag{4}$$

where the damping coefficient d'_e at a discrete event n given by

$$d'_e = \frac{4\pi}{T_0}\zeta_n \qquad , \tag{5}$$

represents the equivalent linear damping. For a discrete time interval $\pm T_{d,n}/4$ around a peak of rotation $\Theta_n(t_n)$ the logarithmic decrement δ_n can then be determined from the decay between the previous and the subsequent peak of oscillation by

$$\delta_n = ln\left(\frac{\Theta_{n-1}}{\Theta_{n+1}}\right) \quad , \tag{6}$$

leading to the instantaneous damping ratio, with

$$\zeta_n = \frac{1}{\sqrt{1 + (\frac{2\pi}{\delta_n})^2}} \qquad . \tag{7}$$

One consequently obtains a set of discrete points of the damping ratio ζ describing the course of the damping with respect to the rotation amplitude and hence implicitly to the velocity.

2 EXPERIMENTAL SETUP

Experimental free decay tests are performed in the wave tank of the Marine Research Group of Queen's University Belfast. Tests are performed with a 40^{th} scale model of a generic box-shaped OWSC with full-scale width of 26m, thickness of 3.5m and height of 12.4m, see figure 1. The model is mounted on a bottom tube pivoted on a steel substructure with hinge depth of 9.5m (full scale). The rotation of the flap is

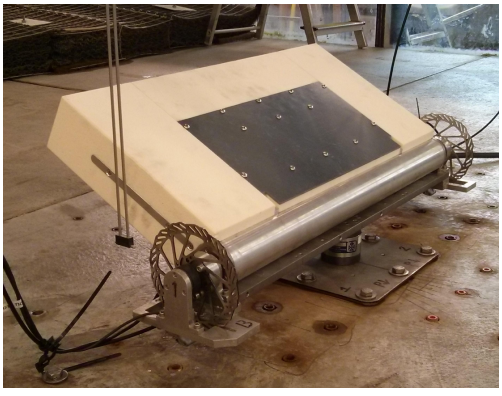

Figure 1: Photograph of 40^{th} scale flap model mounted on bottom tube and substructure.

measured using a Blade Rotary Sensor by Gill Research and Development Ltd. with the sensor being mounted on the substructure and the 'activator' blade rotating with the bottom tube.

Even though no external, non-hydrodynamic damping is applied by the PTO simulation mechanism, torque propagating through the bottom tube is measured using strain gauge torque transducers. Since the model is pitching freely the measured torque is supposed to be measured as zero. Any torque measured is thus related to the residual bearing friction and can be included in the evaluation of the experimental results.

Displacing the model from equilibrium is performed manually.

3 NUMERICAL SETUP

The CFD setup is based on the open source toolbox *OpenFOAM* using the solver *interFOAM*, as presented by Rusche (2002). The solver applies the Eulerian volume of fluid method (VOF) to model the free surface interface as well a k-ω-SST RANS turbulence model, see Menter (1994).

Like the experimental setup, the numerical setup is originally designed to perform simulations with the OWSC being excited by waves and underwent extensive validation in that context (Schmitt 2013). Since a moving body is simulated the mesh has to be adapted in every time step with regard to the change of position of the body. Therefore the mesh consists of a static outer mesh and a moving inner mesh where the outer mesh represents the surrounding wave tank. The base structure of the inner mesh is a cylinder, see figure 2. Its centreline coincides with the hinge axis

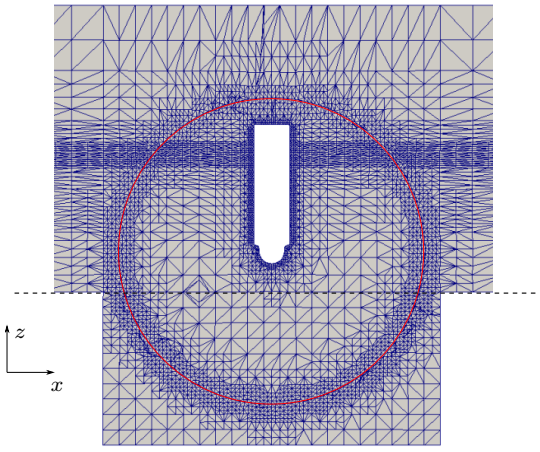

Figure 2: Segment of the mesh (view on the cross-sectional plane in y-direction). Red circle marking the the boundary between static and moving mesh. Dashed line marking the tank floor and boundary for impulse dissipation function.

of the flap which is placed inside of it. The rotation of the cylinder and the included flap is derived from the equation of motion of the flap in every time step. Therefore the resulting hydrodynamic torque is computed from the pressure and viscous shear forces acting on the surface of the flap and their corresponding lever with respect to the hinge axis. The equation of motion as implemented in *OpenFOAM* is given as

$$I \cdot \ddot{\theta} = m \cdot g \cdot CoG \cdot sin(\theta) + \sum_{i=1}^{n} (M_{p,i} + M_{\tau,i}) \quad (8)$$

where m is the mass of the flap and CoG is the length of the perpendicular line from the centre of gravity of the flap to the pivot. $M_{p,i}$ and $M_{\tau,i}$ are the moments due to pressure and viscous shear stress, respectively, related to a cell i on the patch of the flap surface.

Since the hinge height over ground is smaller than the height of the flap the radius of the cylinder exceeds the limits of the tank floor. A rectangular box within the outer mesh is thus placed below the cylinder. To maintain the effect of the presence of the tank floor below the flap a dynamic boundary condition of a three dimensional impulse dissipation function as presented by Clement (1996) is applied to all cells below the actual tank floor. It is represented by an additional dissipative source term $s\rho\vec{U}$ within the the momentum equation of the *interFOAM* solver. Coefficients of the cubic dissipation function s were determined empirically and validated by Schmitt (2013).

The region of the dynamic boundary condition is updated every time step to account for the rotation of the cylinder. The same dissipation function is applied to the front and rear of the tank representing a numerical beach absorbing radiated waves.

The initial position of the OWSC in the free decay test is implemented by rotating the inner cylinder in the preprocessing.

4 VALIDATION

4.1 *Results & Discussion*

As stated in equation 7 the damping ratio ζ during free decay is analysed by means of a discrete value for half a period of oscillation around each peak. To increase the amount of data points (peaks of different rotation amplitudes) several tests are performed with different angles of release, namely four experimental ($\Theta_0 = 18°, 22°, 30°, 52°$) and two numerical ($\Theta_0 = 40°, 90°$). An example plot of the rotation of a numerical and experimental test are shown in figure 3. Note that at the time of writing no tests with coinciding angle of release were performed. However, a validation of the numerical method can be performed as a free decay can be entirely characterised by means of the damped natural period T_d and the damping ratio ζ as a function of the rotation amplitude Θ.

In order to exclude uncertainties due to the manual release of the flap in the experiments the first half oscillation of each test is not included in the evaluation. All peak-wise data points shown in subsequent

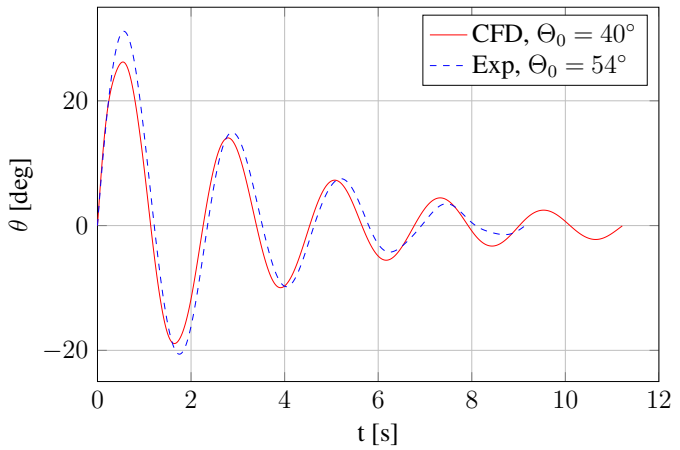

Figure 3: Examples of rotation over time found in the numerical and experimental free decay tests

plots consequently stem from the second and following peaks of each test.

For the purpose of validation the damped natural period $T_{d,n}$ over the rotation amplitude of the corresponding peak Θ_n is compared in figure 4. It shows the peak-wise data found in all physical tests as well as numerical results found within the same range of rotation amplitudes (the decay in the numerical tests showed more oscillations at low rotation amplitudes). A polynomial fit is applied in order to facilitate the comparison.

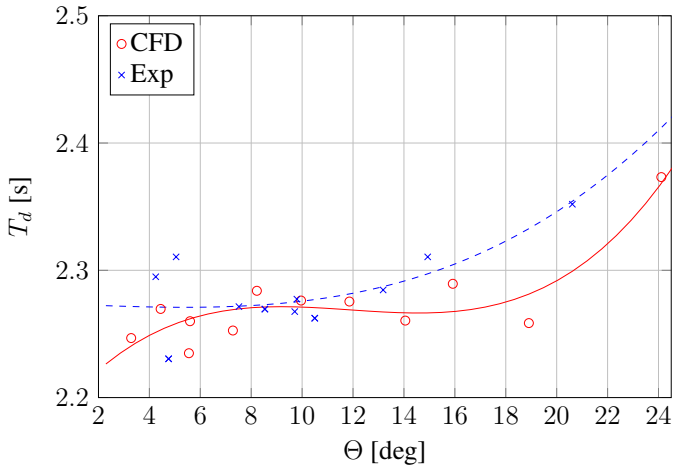

Figure 4: Damped natural period over rotation amplitude

It can seen in figure 4 that the agreement between experiments and numerical simulations is generally good with a mean relative error between the simulations and the experiments of -1.22%, determined from the mean point-wise relative deviation of the polynomial fits. Relative errors are found to be highest at $\Theta > 10°$. Due to the scatter of both, the experimental, and numerical data points further tests providing more peak-wise data points will have to clarify the severity of the deviation. Apart from the damping ratio, implicitly given in the damped natural period, it shows that mass and buoyancy properties as well as the added moment of inertia can be modelled since the undamped natural period, with

$$T_0 = 2\pi\sqrt{\frac{I + I_a}{k_p}} \quad , \tag{9}$$

is also implicitly given in T_d according to equation 2.

Explicitly comparing the instantaneous damping ratio (see figure 5) reveals that the best agreement is found for rotation amplitudes of $\Theta > 10°$ where relative errors lie within a range of -5% to -10%. At lower rotation amplitudes the deviation signifi-

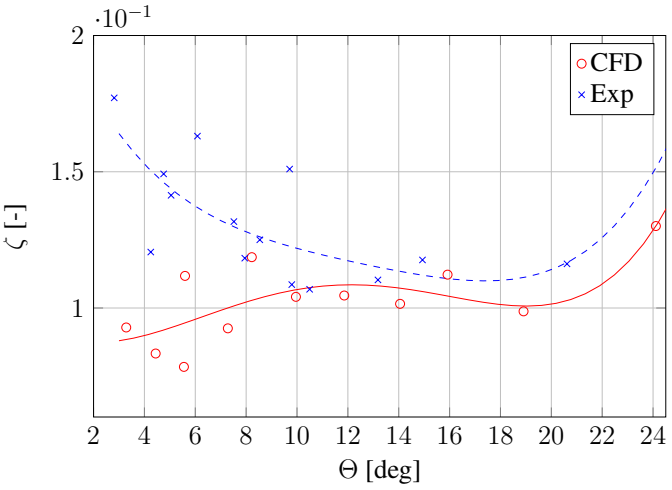

Figure 5: Damping ratio over rotation amplitude

cantly increases. At the point of writing it is assumed that this is related to the occurring external damping torque due to bearing friction in the experiments which is measured as $T_b = 0.08\text{N m}$ RMS. The assumption is based on the fact that the driving restoring moment as well as the overall hydrodynamic damping torque decreases with decreasing rotation amplitude. The influence of the constant bearing friction torque on the damping ratio consequently increases.

The comparison of experimentally and numerically determined damped natural periods and damping ratios shows that the applied CFD setup can model a free decay test. Additionally taking into account previous validations of the numerical model (Schmitt 2013), especially the modeling of viscous effects can assumed to be correct.

5 DETERMINATION OF DAMPING COEFFICIENTS

5.1 *Application of the Faltinsen Method*

A standard method in the offshore industry to determine the linear (d'_r) and quadratic (d'_{nl}) damping coefficients, as given in equation 1, from a free decay test is described by Faltinsen (1990). It determines the dissipation of the potential energy by means of a peak-wise linear damping coefficient (corresponding to d'_e described in section 1.2) by equating it with

the corresponding loss in potential energy given in the linear-quadratic expression, resulting in

$$\frac{2}{T_{d,n}} ln\left(\frac{\Theta_{n-1}}{\Theta_{n+1}}\right) = p_1 + \frac{16\,\Theta_n}{3\,T_{d,n}}\,p_2 \qquad . \tag{10}$$

The coefficients p_1 and p_2, corresponding to d'_r and d'_{nl} respectively, can then be found by plotting the left hand side of equation 10 over $\frac{16}{3}\,\Theta_n/T_{d,n}$ and applying a linear fit.

In preceding investigations of the hydrodynamics of an OWSC (Henry 2009, van't Hoff 2009) the stated method could not be applied successfully since the performed experimental free decay tests did not provide a sufficient number of oscillations. Due to a higher pitch stiffness k_p of the investigated model and a generally prolonged decay in the numerical tests with no residual bearing friction this issue is overcome in this investigation. Figure 6 shows the damping ratio ζ derived from all peak-wise points found in the numerical simulations and the resulting linear fit using the Faltinsen method. Note that the linear fit yielding the equivalent damping coefficient d'_e according to equation 10 is normalised with respect to $T_0/4\,\pi$ in order to obtain ζ. The goodness of fit is measured using the coefficient of determination R^2 and the root mean square error e_{RMS}, see for instance Pardoe (2012).

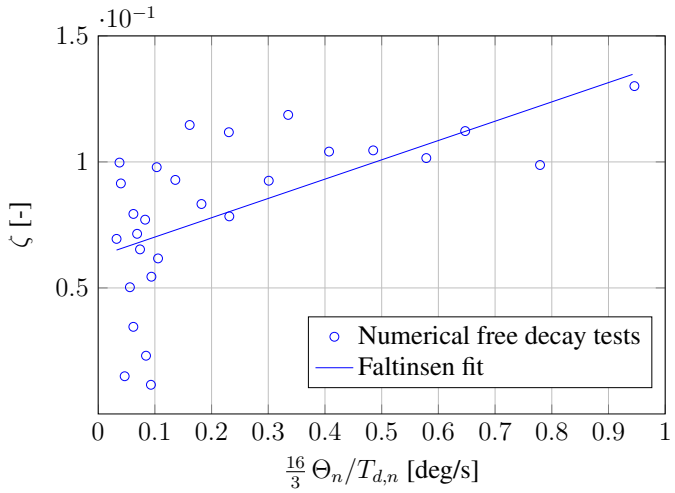

Figure 6: Faltinsen method applied to the numerical free decay data, with $p_1 = 0.0766$ [-] and $p_2 = 0.0625$ [s^{-1}]; $R^2 = 0.356$ [-], $e_{RMS} = 0.258 \cdot 10^{-1}$ [-]

It is found that a linear fit cannot account for the occurring damping characteristic. As the damping ratio is scattered around a constant value of $\zeta = 0.1$ for amplitudes of rotation $\frac{16}{3}\,\Theta_n/T_{d,n} > 0.12$ but increases steeply for $\frac{16}{3}\,\Theta_n/T_{d,n} < 0.1$, only a piecewise applied fit using the Faltinsen method can model the actual damping. Moreover it reveals that the preceding assumption of a linear-quadratic damping for OWSCs generally does not hold.

5.2 *Application of Alternative Methods*

During a free decay in still water we can still assume that damping due to wave radiation is linear (Falnes 2002, Renzi & Dias 2012). The deviation must thus stem from a non-quadratic characteristic of the viscous damping term. Since the assumption of a quadratic viscous damping originates from the drag force acting on bodies in a steady state flow deviations due to the oscillatory motion can actually be expected.

The observations made stand in general agreement with findings in similar offshore applications. A specific example to be mentioned is the roll damping of FPSO (Floating Production Storage and Offloading) hulls. Compared to other ship hulls they show a rather squared than rounded cross sectional area. The free decay of an FPSO in roll is consequently similar to the one of a box-shaped OWSC in pitch. Zeraatgar et al. (2010) found that the linear-quadratic assumption only holds for very small rotation angles where the linear term is actually dominant. It is therefore suggested to apply a cubic instead of a quadratic damping term. For the data found in this investigation a cubic approach or a higher order polynomial one as presented by Froude (1872) might indeed yield a better fit. The plateau as found for $\frac{16}{3}\,\Theta_n/T_{d,n} > 0.12$ though can only be modelled if the order of the polynomial fit is very high. Otherwise the fit will not be able to account for the damping characteristic over the whole range rotation amplitudes. It is thus not considered within this investigation since its application is not practicable especially if less data points are available.

Another approach for FPSO hulls is given by de Oliveira & Fernandes (2014). Starting from the point that a step-wise defined linear fit can represent the found damping characteristic they suggest a continuous hyperbolic tangent function with

$$\zeta(\theta,\dot{\theta}) = \zeta_1 + (\zeta_2 - \zeta_1)\cdot \tanh\left[\alpha\left(\theta^2 + \frac{(T_0\,\dot{\theta})^2}{4\pi^2}\right)\right] \qquad . \tag{11}$$

Figure 7 shows the fit resulting from the hyperbolic method and the data found in this investigation. With a coefficient of determination of $R^2 = 0.449$ the fit proves to be of better quality than the one using the Faltinsen method, especially as the damping ratios at high rotation amplitudes are represented more correctly. The latter states a major improvement since rotation amplitudes of $\Theta > 5°$ represent the domain where OWSCs mainly rotate during operation. However, only an increased number of data points in that domain can ultimately prove the quality of the applied fit functions. Therefore a wider range of tests with different angles of release has to be performed. Concluding from other free decay investigations mentioned in

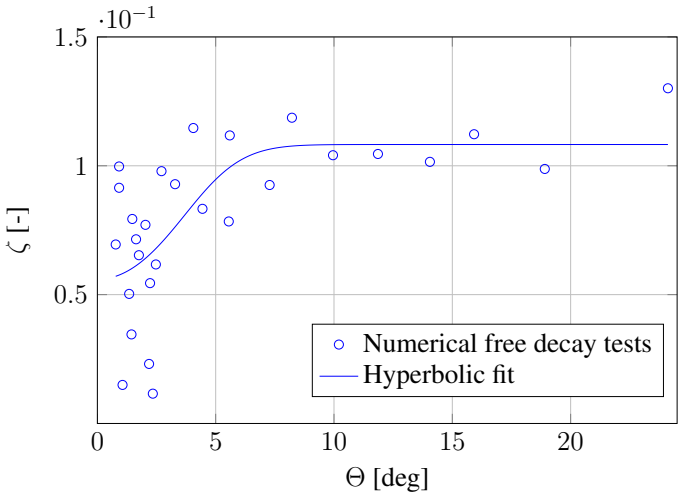

Figure 7: Hyperbolic fit applied to the numerical free decay data, with $\zeta_1 = 0.0559$ [-], $\zeta_2 = 0.00357$ [-] and $\alpha = -0.0381$ [-]; $R^2 = 0.449$ [-], $e_{RMS} = 0.244 \cdot 10^{-1}$ [-]

this section though it is assumed that the better quality of the hyperbolic fit will be corroborated.

5.3 *Implementation into Power Prediction Models*

Finding a better adapted mathematical description of the damping found in the free decay tests is one major step towards an accurate modelling of the hydrodynamic damping of OWSCs. The implementation into power prediction models though also requires the inclusion of the differences in the near flow field between a free decay test and the actual operation in ocean waves. For most offshore structures the latter is straightforward since differences in the relative fluid motion around the body between a free decay test and the motion of water particles in ocean waves are assumed to be small. This is due to the fact that the body's dimensions are usually large relative to the height and length of incident waves. Furthermore the body is only damped by the fluid itself. Both assumptions do not hold for OWSCs. Especially the application of an external non-hydrodynamic damping by the PTO system changes the near-flow field during operation significantly compared to a free-decay test without external damping.

During free decay we can assume that the velocity of the OWSC directly corresponds to the relative fluid velocity around the device since the fluid itself is not moving. When the device is excited by waves and damped by the PTO system this is not the case. Any hydrodynamic damping given as a function of the velocity of the device is thus only applicable as a function of the relative fluid velocity around the device during operation. However, determining the relative fluid velocity is not straightforward.

The only velocity reference in the power prediction model is the absolute fluid velocity in the far field. It can be determined using the analytical description of the incident wave. Furthermore the rotation (amplitude and phase angle) of the device is given as the response of the device to the incident wave, computed with the model itself.

Compared to the far field though, the fluid velocity can change significantly in the near flow field. Memory effects due to the oscillatory motion of the device and the diffraction of incoming waves must also be considered. The diffraction is again dependent on the incident wave, the applied external PTO damping, the response (rotation amplitude and phase angle) and shape of the OWSC. As simple power prediction models do not capture the surrounding fluid explicitly an additional term approximating the relative fluid velocity is required. Only if such can be provided damping coefficients determined from free decay tests can be correctly implemented in existing efficient models. One thereby has to keep in mind that the implementation of a velocity dependent function into the model implies that the motion of the OWSC cannot be solved directly anymore as the hydrodynamic damping and the flap velocity are cross-coupled.

CFD simulations of PTO damped OWSC in operational sea states can yield explicit descriptions of the near flow field fluid velocities. They can thus play a crucial role in future investigations.

6 CONCLUSION

This paper presents the ongoing work upon the determination of non-linear and linear damping coefficients of flap-type OWSCs moving in pitch. Ultimately, their determination is crucial in order to accurately model the annual power production of the device. Numerical free decay tests using an *OpenFOAM* based CFD setup are validated against experimental tests. Furthermore existing methods to determine damping coefficients from free decay test results are applied and put into perspective with respect to their applicability to OWSCs. The major findings are given in the following:

- The presented CFD setup can model the free decay of an OWSC. Its application is not affected by experimental uncertainties leading to more oscillations at low rotation amplitudes. Deviations found at low rotation amplitude are assumed to be related to the experimental set-up.

- Against preceding investigations it is shown that a free decay test can provide a sufficient number of oscillations in order to determine the damping characteristic of the device.

- A model based on linear and quadratic coefficients, as implemented in existing descriptions of an OWSC's hydrodynamic response, cannot accurately model the occurring damping within the whole regime of rotation amplitudes.

- The hyperbolic tangent approach provides a better fit of the hydrodynamic damping.

Further to the hydrodynamical findings the investigation reveals that numerical free decay tests offer several general advantages compared to experimental ones:

- Uncertainties due to the experimental setup are reduced, as for instance bearing friction or slightly imbalanced physical models (small experimental rotations were found to oscillate around $\theta \neq 0°$).
- Reflected radiated waves contaminating experimental results are eliminated by a perfectly absorbing numerical beach.
- The expenditure of human labor to perform a test is immensely reduced if the necessary preprocessing is adequately automated. The effort to test OWSCs of different shape, dimension or operational water level is consequently low.

6.1 *Future Work*

The hyperbolic tangent fit appears to be a good description of the actual damping found in the free decay tests. It can thus serve as a starting point for an improved description of the hydrodynamic damping of OWSCs. Before finally evaluating its accuracy and possibly adjusting the mathematical formulation more free decay tests should be carried out in order to increase the number of data points.

After all, any final damping term then has to be implemented into the time domain model validating it against the original free decay tests. Furthermore simulations using the CFD set-up should be performed implementing the residual bearing friction found in the physical tests. Doing so will provide an improved validation of the numerical tool and allow a better identification of errors in the numerical model.

Most importantly a description of the relative flow velocity around the device as a function of the incident wave height and period and the motion of the PTO damped flap itself has to be found. Analytical or empirical descriptions can be compared against CFD simulations of the device during operation providing insight into the details of the near flow field. It can be assumed that errors in the description of the relative flow velocity are negligible in a certain range of operational sea states. As the damping characteristic found in the free decay tests is scattered around a constant value for rotation amplitudes of $\Theta > 8°$ the occurring hydrodynamic damping may also be invariant to the corresponding relative velocity.

REFERENCES

Bhinder, M., A. Babarit, L. . Gentaz, & P. Ferrant (2012). Effect of viscous forces on the performance of a surging wave energy converter. *Proceedings of the Twenty-second International Offshore and Polar Engineering Conference, Rhodes, Greece, June 17 - 22*.

Clement, A. (1996). Coupling of two absorbing boundary conditions for 2d time domain simulations of free surface gravity waves. *Journal of Computational Physics 162*, 139 – 151.

de Oliveira, A. & A. Fernandes (2014). The nonlinear roll damping of a FPSO hull. *Journal of Offshore Mechanics and Arctic Engineering 136*, 1 – 10.

Falnes, J. (2002). *Ocean Waves and Oscillating Systems*. Cambrigde University Press.

Faltinsen, O. (1990). *Sea Loads on Ships and Offshore Sturctures*. Cambridge University Press.

Faltinsen, O. (2010). *Hydrodynamics of High-Speed Marine Vehicles*. Cambridge University Press.

Folley, M., B. Elsaesser, & T. Whittaker (2009). Analysis of the wave energy resource at the european marine energy centre. *9th International Breakwater Conference, UK, Edinburgh*.

Froude, W. (1872). On the influence of resistance upon the rolling of ships. *Naval Science* (1), 411 – 429.

Henry, A. (2009). *The hydrodynamics of small seabed mounted bottom hinged wave energy converters in shallow water*. Ph. D. thesis, Queen's University Belfast.

Ikeda, Y. (1983). On the form of nonlinear roll damping of ships: a technical note. *Bericht, Institut für Schiffs- und Meerestechnik, Technische Universität Berlin* (15).

Inman, D. (2008). *Engineering Vibrations*. Pearson.

Menter, F. R. (1994). Two-equation eddy-viscosity turbulence models for engineering applications. *AIAA Journal 32*, 1598 – 1605.

Osterried, M. (2010). *Power from waves: Oscillating Wave Surge Converters in the near-shore region*. Ph. D. thesis, Queen's University Belfast.

Pardoe, I. (2012). *Applied Regression Modeling: A Business Approach*. John Wiley & Sons.

Renzi, E. & A. Dias (2012). Hydrodynamics of the oscillating wave surge converter in the open ocean. *European Journal of Mechanics B/Fluids 41*, 1 – 10.

Rusche, H. (2002). *Computational Fluid Dynamics of Dispersed Two-Phase Flows at High Phase Fractions*. Ph. D. thesis, Imperial College London.

Schmitt, P. (2013). *Investigation of the near flow field of bottom hinged flap type wave energy converters*. Ph. D. thesis, Queen's University Belfast.

Schmitt, P., T. Whittacker, D. Clabby, & K. Doherty (2012). The oppurtunities and limitations of using CFD in the developement of waver energy converters. *RINA Marine & Offshore Renewable Energy Conference, London*.

van't Hoff, J. (2009). *Hydrodynamic modelling of the Oscillating Wave Surge Converter*. Ph. D. thesis, Queen's University Belfast.

Zeraatgar, H., M. Asghari, & F. Bakhtiari-Nejad (2010). A study of the roll motion by means of a free decay test. *Journal of Offshore Mechanics and Arctic Engineering 132*.